

Electric Double-layer Capacitance and Pseudocapacitance Contributions to the Oxidative Modification of Helical Carbon Nanofibers

Yong Gong^{1,2}, Xian-Guang Zeng², Tong Luo², Zu-Yang Dai², Yong-Zhong Jin², Jian Chen², Yong Yi¹, Tao Duan¹, Yong-Jian Tang^{1*}

¹ State Key Laboratory of environment-friendly energy materials, Southwest University of Science and Technology, Mianyang, 621010, China

² Material Corrosion and Protection Key Laboratory of Sichuan province, Sichuan University of Science and Engineering, Zigong, 643000, China

*E-mail: tangyongjian2000@sina.com (Yong-Jian Tang)

Received: 17 April 2020 / Accepted: 8 June 2020 / Published: 10 July 2020

Surface functionalization with oxygen-containing functional groups of helical carbon nanofibres (HCNFs) is a simple and effective method to increase the capacitive performance of the HCNFs. However, the contribution of the electric double-layer capacitance (EDLC) and pseudocapacitance (PC) to the overall behaviour of supercapacitors has not yet been explored. A HNO₃ treatment and the modified Hummers method were used to increase the oxygen-containing functional groups and specific surface area of the HCNFs. The increase in the specific surface area enhanced the EDLC, while the oxygen-containing functional groups led to PC. As a result of the modified Hummers method, the HCNFs with a specific surface area of 78.82 m²/g and containing 28.03 at.% oxygen had a specific capacitance of 143.6 F/g at 1 A/g, which is much higher than that of the pristine HCNFs (10.7 F/g). In addition, the contribution of the EDLC and PC were evaluated and are discussed.

Keywords: Helical carbon nanofibers, pseudocapacitance, electric double-layer capacitance, oxidative modification

1. INTRODUCTION

HCNFs have aroused widespread research interest due to their unique helical structure in recent years. They have shown incredible potential for reinforcing composites [1, 2] and for application in electrochemical sensors [3, 4], microwave absorbers [5, 6], and supercapacitors [7-10]. The formation of the helical structure can increase the surface area of HCNFs, which store potential energy for capacitors. Childress et al. reported a specific capacitance of 125.0 F/g at 3 mV/s for asymmetric

capacitors made from helically coiled carbon nanotubes [7]. Cheng et al. found that the specific capacitance of HCNFs is 9.2 F/g at 100 mA/g, which is much higher than that of straight carbon fibres [10]. Acidified HCNFs showed a high specific capacitance of 95 F/g at 0.1 A/g by Zeng et al. [8]. The results showed that the helical structure of HCNFs can significantly increase the specific surface area, which can improve the specific capacitance effectively.

Despite the presence of several reports on the electrochemical performance of HCNFs in the literature, the effective enhancement of electrochemical properties for supercapacitors remains a tremendous challenge. In recent years, a substantial amount of effort has been made to increase the specific capacitance of carbon-based materials. Surface oxidation is the most frequently used method, among which oxygen oxidation [11], nitric and sulfuric acid oxidation [12, 13], plasma oxidation [14] and ozone oxidation [15] are used most frequently. The application of these treatments to carbon-based materials increased their specific surface area and oxidized functional groups [11, 16]. Oxidized carbon-based materials have two mechanisms to improve their specific capacitance: PC, which is attributed to oxidative functional groups, and EDLC, which is attributed to the increased specific surface area [17-19]. Unfortunately, few efforts have been made to discern the actual contribution of the EDLC and PC in oxidized carbon-based materials on the capacitance [20, 21].

In this work, two kinds of oxygen-containing HCNFs were modified by HNO₃ treatment and the modified Hummers method. The effects of the microstructure and oxygen-containing functional groups on the capacitance were studied after modification. The contributions of the EDLC and PC were evaluated and are discussed.

2. EXPERIMENTAL METHODS

2.1. Chemicals

The HCNFs were prepared by the chemical vapor deposition method as described in our previous work [22]. KMnO₄ (AR), KOH (AR), 68% HNO₃, 98% H₂SO₄, and 30% H₂O₂ were purchased from Kelong Chemical Reagent Crop. Chengdu, China. All chemical reagents were used without further purification.

2.2. Oxidation of the HCNFs

The oxidized HCNFs were prepared by a facile HNO₃ method and modified Hummers method [23, 24]. The HCNFs (1 g) were mixed with 90 mL H₂SO₄ and 30 mL HNO₃ and then ultrasonicated at 210 W for 60 min. Then, the reaction solution was placed in an ice-water bath at 0 °C for 4 h with stirring. Then, 2 g KMnO₄ was slowly added and stirred for 4 hours. Another 50 mL of deionized water was incorporated along with 5 mL of H₂O₂ solution. The obtained suspension was filtered, washed with deionized water until the pH level was neutral, and finally dried at 80 °C for 24 h. The obtained HCNFs sample that was treated with the modified Hummers method was labelled HCNFs-2.

For comparison, 1 g HCNFs was mixed with 100 mL HNO₃ and ultrasonicated at 210 W for 60 min. The obtained sample was labelled HCNFs-1.

2.3. Materials Characterization

The morphologies were observed with field emission scanning electron microscopy (FESEM, Thermo Fisher Quattro C, USA) and high-resolution transmission electron microscopy (HRTEM, JEM-2001F, Japan). The crystal structure was characterized by X-ray diffraction (XRD, D8 Advance, Bruker, Germany). The specific surface area and pore size distribution were calculated by the Brunauer-Emmett-Teller (BET, ASAP 2460, Micromeritics, USA) technique. Various surface functional groups were measured by using Fourier transform infrared (FTIR, Nicolet 6700, Thermo Fisher Scientific, USA) spectrometry and X-ray photoelectron spectroscopy (XPS, ESCALAB250Xi, Thermo Scientific, USA).

2.4. Electrochemical Measurements

The experiments were carried out in a three-electrode system. The electrochemical tests were performed on a CHI660E electrochemical workstation using 6.0 M KOH electrolyte solution. A saturated calomel electrode and Pt wire served as the reference and counter electrodes, respectively. The active material, polytetrafluoroethylene and conductive carbon black at a mass ratio of 8:1:1 in N-methylpyrrolidone were mixed homogeneously. Then, the samples were spread onto a 10 mm × 10 mm sized nickel foam and dried under vacuum as the working electrode. Electrochemical impedance spectroscopy (EIS) spectra were obtained in the frequency range from 0.01 Hz to 100 kHz. Cyclic voltammograms (CV) and galvanostatic charge-discharge (GCD) were performed over a voltage range from -0.1 to 0 V.

3. RESULTS AND DISCUSSION

The morphologies of the HCNFs, HCNFs-1 and HCNFs-2 are observed by FESEM and HRTEM. As shown from Figure 1 (a, b, c, d, e, and f), the HCNFs show a high purity, uniform helical morphology and diameter of approximately 100 nm. It is obvious that the morphology and size of the HCNFs in the HCNFs-1 and HCNFs-2 samples do not change significantly, suggesting that the morphology of the HCNFs in the HCNFs-1 and HCNFs-2 samples is not influenced by the HNO₃ treatment and modified Hummers method. Furthermore, as shown in Figure 1 (g, h, and i), HRTEM characterization reveals that all samples have a short-range order graphite layer and an amorphous layer.

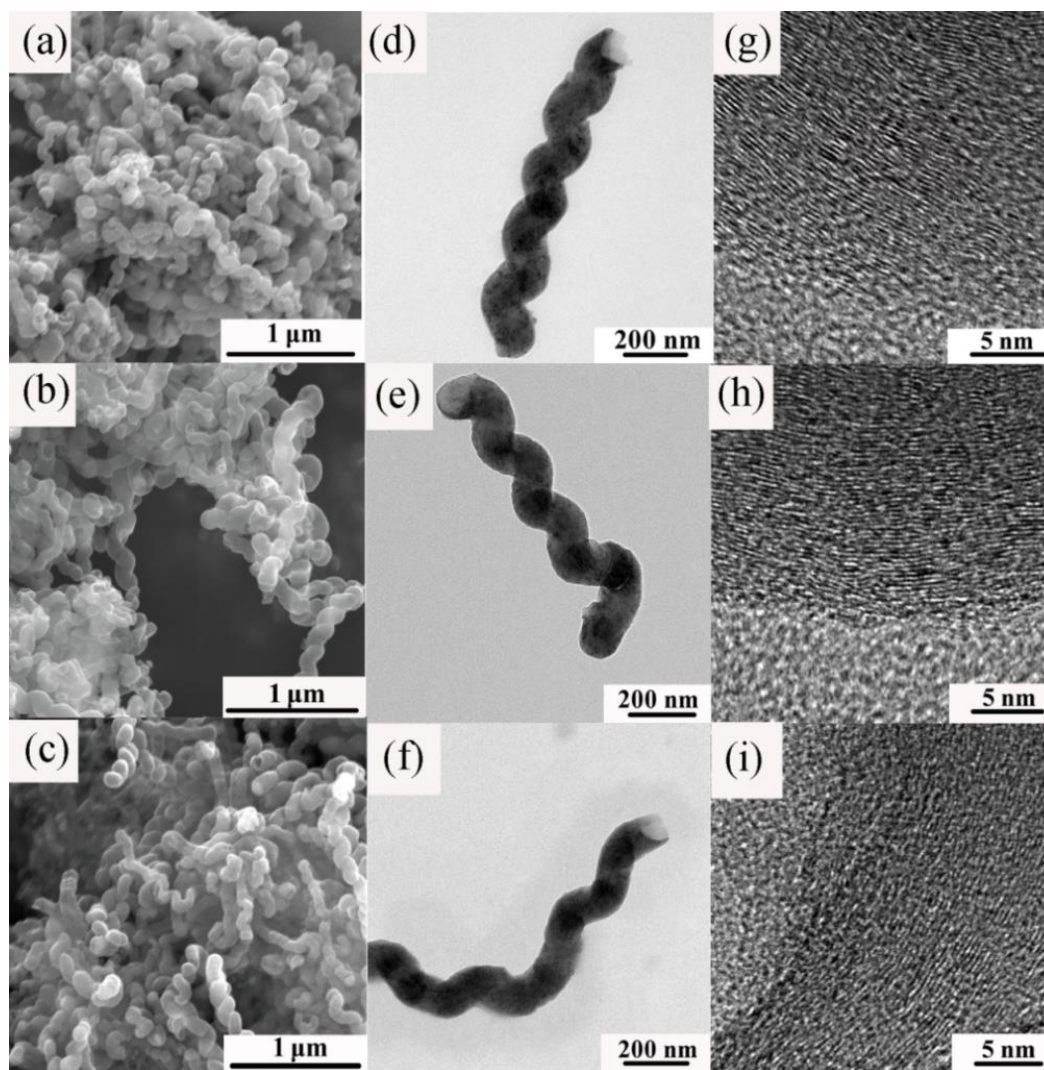


Figure 1. FESEM images of (a) HCNFs, (b) HCNFs-1, and (c) HCNFs-2 samples. HRTEM images of (d) and (g) HCNFs, (e) and (h) HCNFs-1, and (f) and (i) HCNFs-2 samples.

Figure 2a shows the XRD patterns of the HCNFs, HCNFs-1 and HCNFs-2 samples. The XRD patterns of the HCNFs-1 and HCNFs-2 samples are similar to that of the HCNFs, suggesting that oxidation does not change the crystal structure. The characteristic diffraction peaks at 2θ values of approximately 25.7° and 43° correspond to the (002) and (100) crystallographic planes, respectively [12, 16]. Furthermore, XRD patterns of the HCNFs, HCNFs-1 and HCNFs-2 samples present a broad diffraction peak over the range from 10° to 20° , which indicates that all samples have an amorphous layer [25, 26]. The XRD results showed that the HCNFs have a graphite layer and an amorphous layer, which is consistent with the HRTEM characterization.

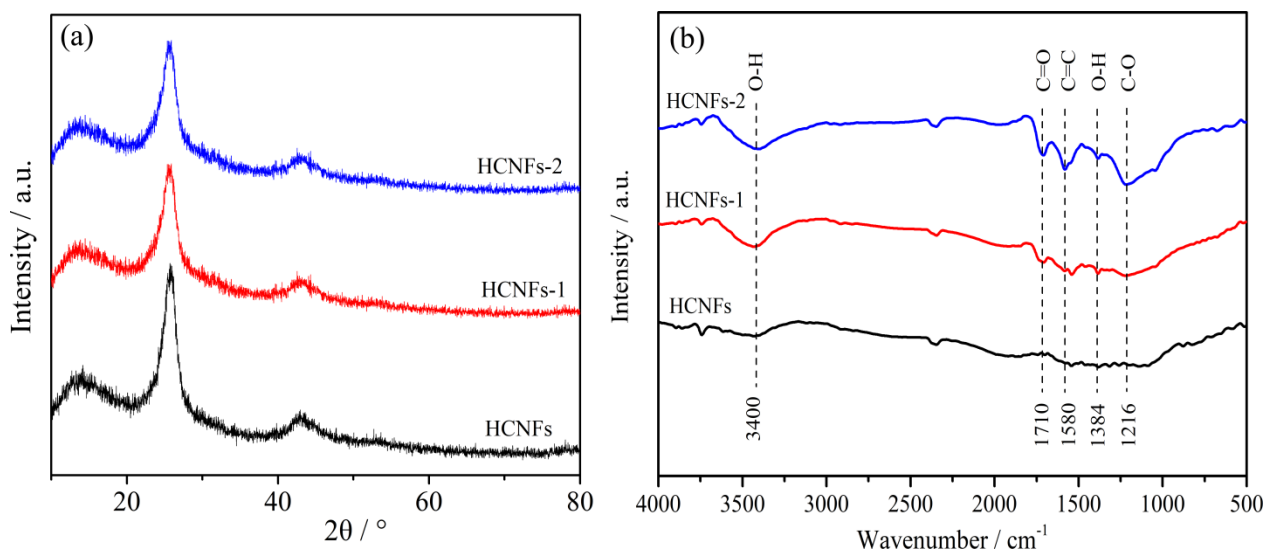


Figure 2. XRD patterns and FTIR spectra of the HCNFs, HCNFs-1 and HCNFs-2 samples.

Table 1. S_{BET} , V_t and average pore sizes of the HCNFs, HCNFs-1 and HCNFs-2 samples.

Sample	$S_{\text{BET}}/(\text{m}^2 \cdot \text{g}^{-1})$	$V_t/(\text{cm}^3 \cdot \text{g}^{-1})$	Average pore size/(nm)
HCNFs	31.73	0.138	8.15
HCNFs-1	73.07	0.283	6.85
HCNFs-2	78.82	0.268	6.65

The HNO_3 treatment and modified Hummers method can significantly affect the surface chemical environment of the HCNFs in all samples herein. As shown in Figure 2b, the FTIR spectra of the HCNFs, HCNFs-1 and HCNFs-2 samples are quite different. For all samples, two weak peaks at 1580 cm^{-1} and 1384 cm^{-1} correspond to peaks from the aromatic C=C vibration and vibration adsorption peak of O–H, respectively [27, 28]. The characteristic peaks indicating oxygen-containing functional groups are observed for the functionalized HCNFs-1 and HCNFs-2 samples. Three intense absorption bands can be seen at approximately 3400 cm^{-1} , 1710 cm^{-1} and 1216 cm^{-1} in the HCNFs-1 and HCNFs-2 samples but were almost absent for the untreated HCNFs. According to references [18, 29, 30], the bands at 3400 cm^{-1} , 1710 cm^{-1} and 1216 cm^{-1} correspond to O–H stretching (hydroxyl), C=O stretching (carbonyl or carboxyl), and the stretching vibration of C–O in COOH, respectively. By the above treatment process, oxygen-containing functional groups are introduced on the surface of the HCNFs. The oxygen-containing functional groups (for example –OH, C–O, COOH) are also confirmed from the binding energy shift observed in the XPS measurements.

The specific surface area (S_{BET}), total pore volumes (V_t) and average pore sizes of the HCNFs, HCNFs-1 and HCNFs-2 samples are listed in Table 1. The S_{BET} increased in the order of HCNFs < HCNFs-1 < HCNFs-2. The S_{BET} and V_t for the HCNFs are $31.73 \text{ m}^2/\text{g}$ and $0.138 \text{ cm}^3/\text{g}$, respectively. The S_{BET} and V_t for the HCNFs-1 sample are $73.07 \text{ m}^2/\text{g}$ and $0.283 \text{ cm}^3/\text{g}$, respectively, while those for the HCNFs-2 sample are $78.82 \text{ m}^2/\text{g}$ and $0.268 \text{ cm}^3/\text{g}$, respectively. Therefore, the oxidation treatments increase the S_{BET} and V_t .

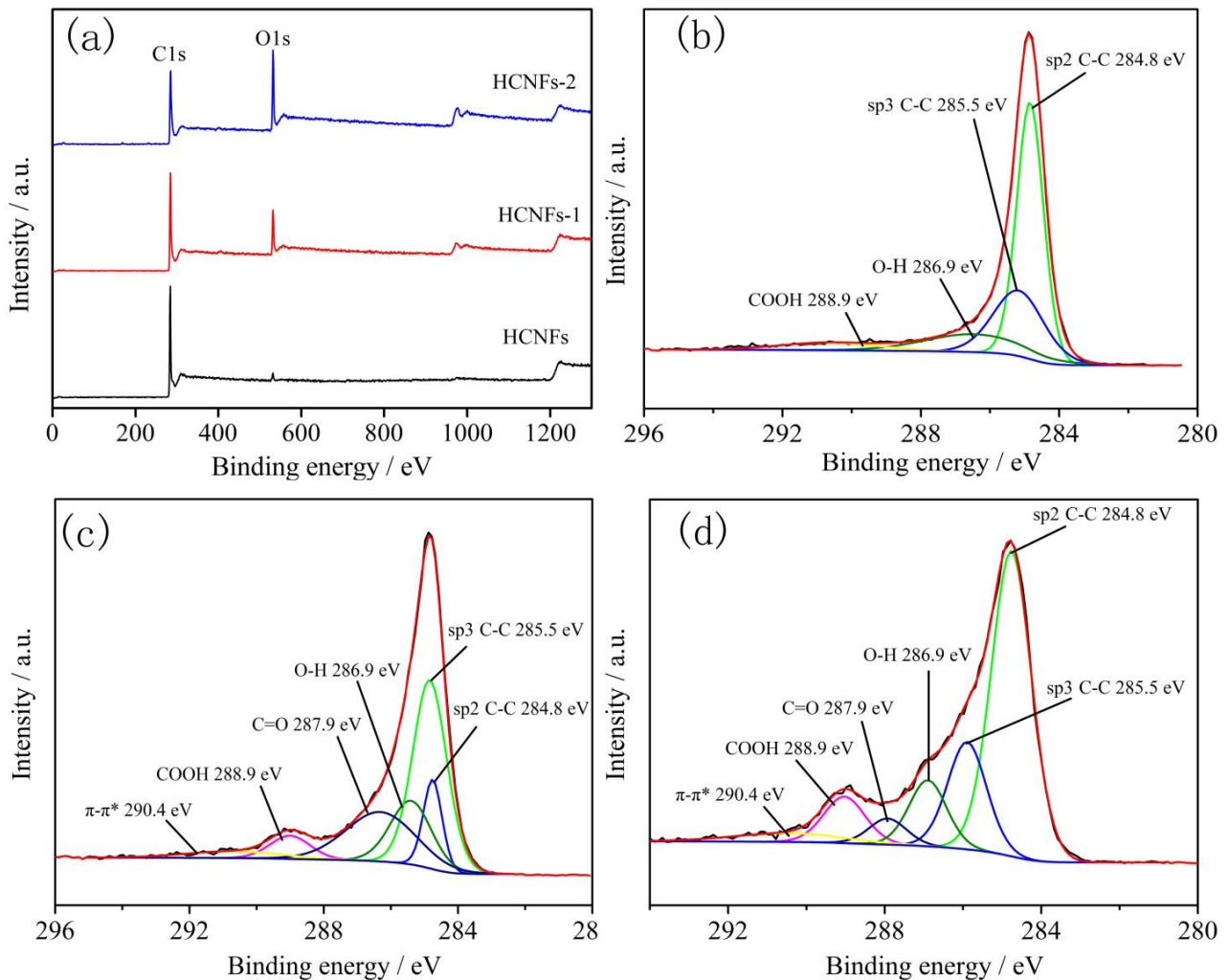


Figure 3. (a) XPS wide scan survey spectra of the HCNFs, HCNFs-1 and HCNFs-2 samples, (b) C1s of the HCNFs, (c) C1s of the HCNFs-1 sample, and (d) C1s of the HCNFs-2 sample.

Table 2. XPS elemental analysis of the HCNFs, HCNFs-1 and HCNFs-2 samples.

Sample	C1s (at.%)	O1s (at.%)	O-H (at.%)	C=O (at.%)	COOH (at.%)
HCNFs	96.23	3.77	2.64	-	1.13
HCNFs-1	83.45	16.55	6.19	8.15	2.21
HCNFs-2	71.97	28.03	12.92	5.08	10.03

XPS is performed to understand the changes in the oxygen-containing functional groups on the surfaces of all samples. The elements of carbon and oxygen are detected in the survey spectra, as shown in Figure 6a. It is obvious that the oxygen content of the HCNFs increases with HNO_3 treatment and the modified Hummers method. As shown in Table 2, the percentage of oxygen atoms increases from 3.77% to 16.55% and 28.03%. The degree of oxidation is further investigated using the C1s spectrum of the HCNFs, HCNFs-1 and HCNFs-2 samples in Figure 6b-d. Compared to that for the

HCNFs, the C1s spectra of the HCNFs-1 and HCNFs-2 samples showed six components at 284.8, 285.7, 286.9, 287.7, 289.03 and 290.6 eV, corresponding to the sp² C–C, sp³ C–C, O–H, C=O, COOH and π – π^* transitions[17, 31], respectively. Table 2 shows the relative content for each peak of the C1s spectra. The relative contents of O–H, C=O, and COOH in the HCNFs-2 sample are all higher than those in the HCNFs and HCNFs-1 sample. The higher content of oxygen-containing functional groups is expected to increase the contribution from the PC.

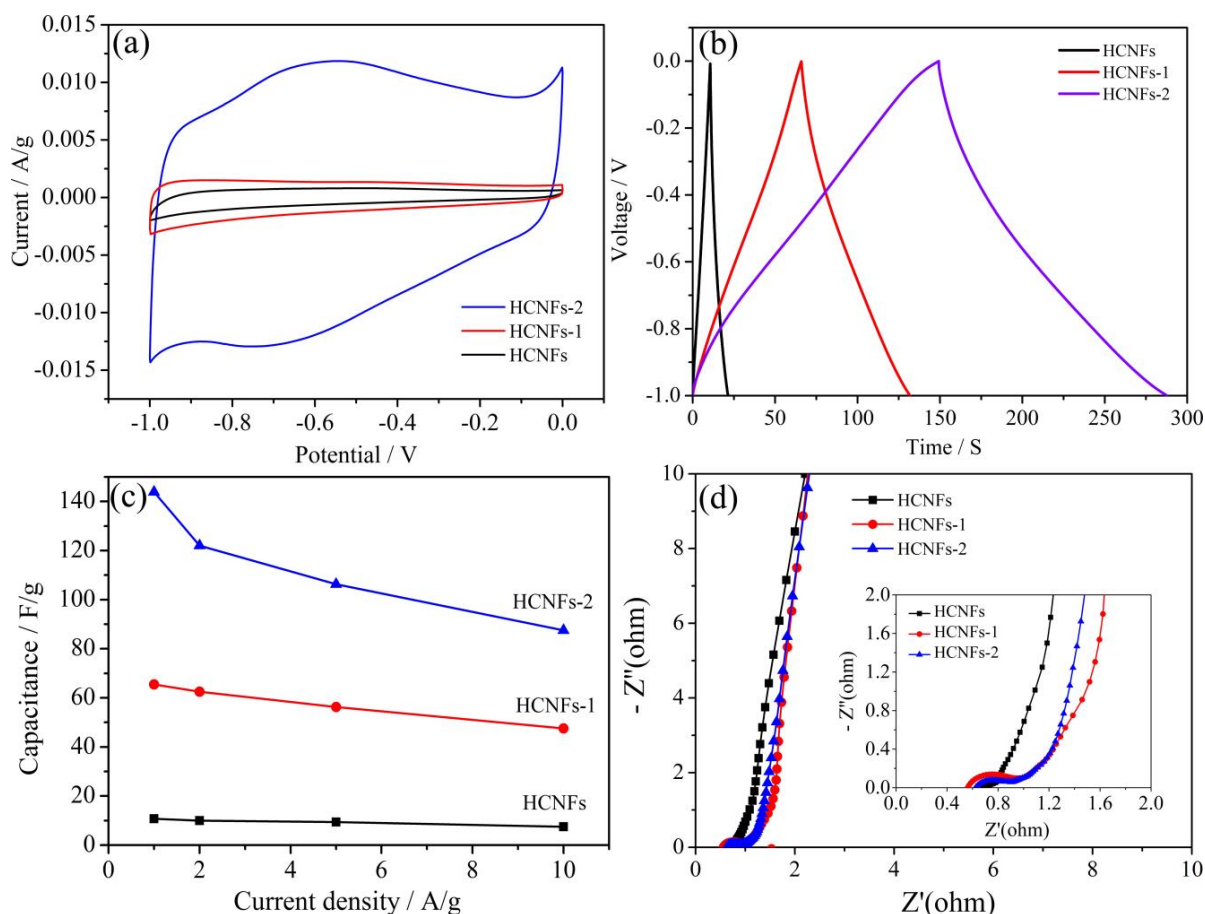


Figure 4. (a) CV curves of all samples at 10 mV/s, (b) GCD curves of all samples at 1 A/g, (c) capacitance with respect to current density for all samples, and (d) EIS of all samples.

Figure 4a shows the CV results for the HCNFs, HCNFs-1 and HCNFs-2 electrodes in 6 M KOH electrolyte. In Figure 4a, the CV curves of the HCNFs and HCNFs-1 electrodes show approximately rectangular-like shapes. Apparently, the HCNFs-2 electrode shows the largest CV area corresponding to the highest specific capacitance. In addition, the HCNFs-2 electrode presents a pair of obvious camel-shaped redox peaks between -0.8 and -0.5 V, indicating the pseudocapacitive Faradaic redox reaction with carboxyl and hydroxyl groups. This is confirmed by the GCD curves shown in Figure 4b. As indicated in Figure 4b, all of the GCD curves generally have a nearly triangular shape, suggesting excellent capacitive behaviour. The charge-discharge time of HCNFs-2 is much longer than that of HCNFs and HCNFs-1, which implies that HCNFs-2 possessed a higher

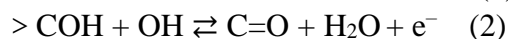
specific capacitance value. Unsurprisingly, the GCD curves of HCNFs-2 show a slight bend during discharging due to the faradic reactions caused by the presence of oxygen functional groups.

Figure 4c shows the gravimetric specific capacitances of all samples that were calculated from the GCD curves at different current densities. At a current density of 1 A/g, the specific capacitance of HCNFs-2 calculated based on the discharge curves reaches 143.6 F/g, which is larger than the value of 65.5 F/g for the HCNFs-1 sample and 10.7 F/g for the HCNFs sample. Many studies have reported various electrode materials with helical morphologies for supercapacitors. To demonstrate the excellent electrochemical performance of the HCNFs-2 electrode, a comparison of electrode materials with a helical morphology for supercapacitors is listed in Table 3. Evidently, the HCNF-2 electrode in this work exhibits a higher capacitance than the other carbon-based materials in the list.

Table 3. Comparison of electrode materials with a helical morphology for supercapacitors.

Electrode materials	Electrolyte	Capacity (F/g)	Reference
Coiled carbon nanotubes	1 M Et ₄ NBF ₄ /AN	125.0 (3 mV/s)	[7]
HCNFs	1 M Na ₂ SO ₄	95.0 (0.1 A/g)	[8]
Micro-coiled carbon fibres	6 M KOH	9.2 (0.1 A/g)	[10]
Carbon nanocoils	3 M KOH	40.25 (1 mA)	[32]
Coiled carbon nanotubes	0.5 M H ₂ SO ₄	51.29 (0.125 A/g)	[33]
Coiled carbon nanotubes	5 M KOH	125.7 (300 mV/s)	[34]
HCNFs-2	6 M KOH	143.6 (1 A/g)	This work

The HCNFs-1 and HCNFs-2 electrodes show a higher capacitance than that of the HCNFs electrode because they have a large increase in the specific surface area, total pore volume, and oxygen-containing functional groups. Obviously, the synergistic effect of the EDLC and PC in the HCNFs-1 and HCNFs-2 samples greatly improves their electrochemical performances. In 6 M KOH electrolyte, the Faraday redox reactions of the carboxyl and hydroxyl groups are described by equations (1) and (2), respectively[35, 36]:



The EIS analyses of all samples are performed over a frequency range from 0.01 Hz-100 kHz with an AC amplitude of 10 mV, as shown in Figure 4d. The high-frequency region of the spectra is shown in the inset image. The HCNFs sample show an almost vertical line in the low-frequency band and no semicircle in the high-frequency band [37]. The HCNFs-1 and HCNFs-2 samples show a semicircle at high frequencies, which is related to the charge transfer process; it specifically represents the electron transfer limit process, and its effective diameter is equal to the Faraday charge transfer resistance [38]. The line with a slope of 45° in the medium-frequency region for the HCNFs-1 and HCNFs-2 samples corresponds to the Warburg impedance, which is caused by the frequency dependence of the ion diffusion/transmission processes in the electrolyte [39]. The nearly vertical line in the low-frequency band for the HCNFs-1 and HCNFs-2 samples indicates ideal capacitive behaviour and a low diffusion resistance of ions in the electrolyte [40]. The internal resistance (R_s) is the intercept with the X-axis. R_s is generated by the internal resistance of the active substance, the

electrode and the electrolyte in the separator, and the contact resistance in the system [41, 42]. Moreover, the R_s values of the HCNFs, HCNFs-1 and HCNFs-2 are 0.85 Ω , 0.58 Ω and 0.72 Ω , respectively.

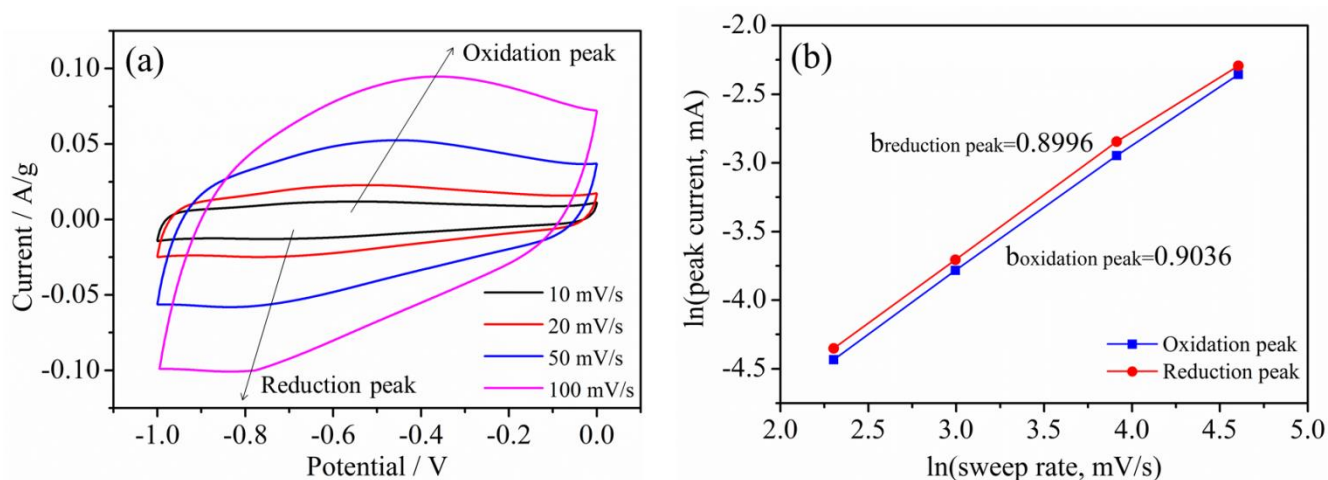


Figure 5. (a) CV curves of HCNFs-2 at scan rates from 10 to 100 mV/s, (b) linear relationship of $\ln i$ versus $\ln v$ at the oxidation peak and reduction peak, where the b value is the fitted-line slope.

As shown in Figure 5a, the CV curves of HCNFs-2 at various scan rates displayed a roughly rectangular shape, showing that the EDLC is the major contribution to overall energy storage. The CV maintains the quasi-rectangular shape at 100 mV/s, indicating that HCNFs-2 can store additional energy through a fast ion adsorption mechanism and has a good rate performance. After surface modification with the HNO_3 treatment and the modified Hummers method, the specific surface areas and the oxygen functional groups are responsible for the increase in the capacitance. Generally, a high specific surface area can increase the EDLC, and the oxygen-containing functional groups by reversible faradic reactions (PC) can improve the specific capacitance. According to the current-response characteristics, the current response at a specific voltage can be obtained by equations (3) and (4) [43]:

$$i = a v^b \quad (3)$$

$$\ln i = \ln a + b \ln v \quad (4)$$

where i is the peak current, v is the scan rate, and a is an empirical parameter. When the b value is 0.5, the electrode shows diffusion-controlled redox control (a PC feature), and when the b value is 1, the electrode shows a non-diffusion-controlled surface capacitive process (an EDLC feature). Figure 5b shows the b values of the oxidation peak and reduction peak for HCNFs-2 as deduced from the slope of the $\ln i$ versus $\ln v$ curves, which are 0.9036 and 0.8996, respectively. The b values of the oxidation peak and reduction peak imply that the HCNFs-2 sample mainly exhibits EDLC-controlled kinetics behaviour.

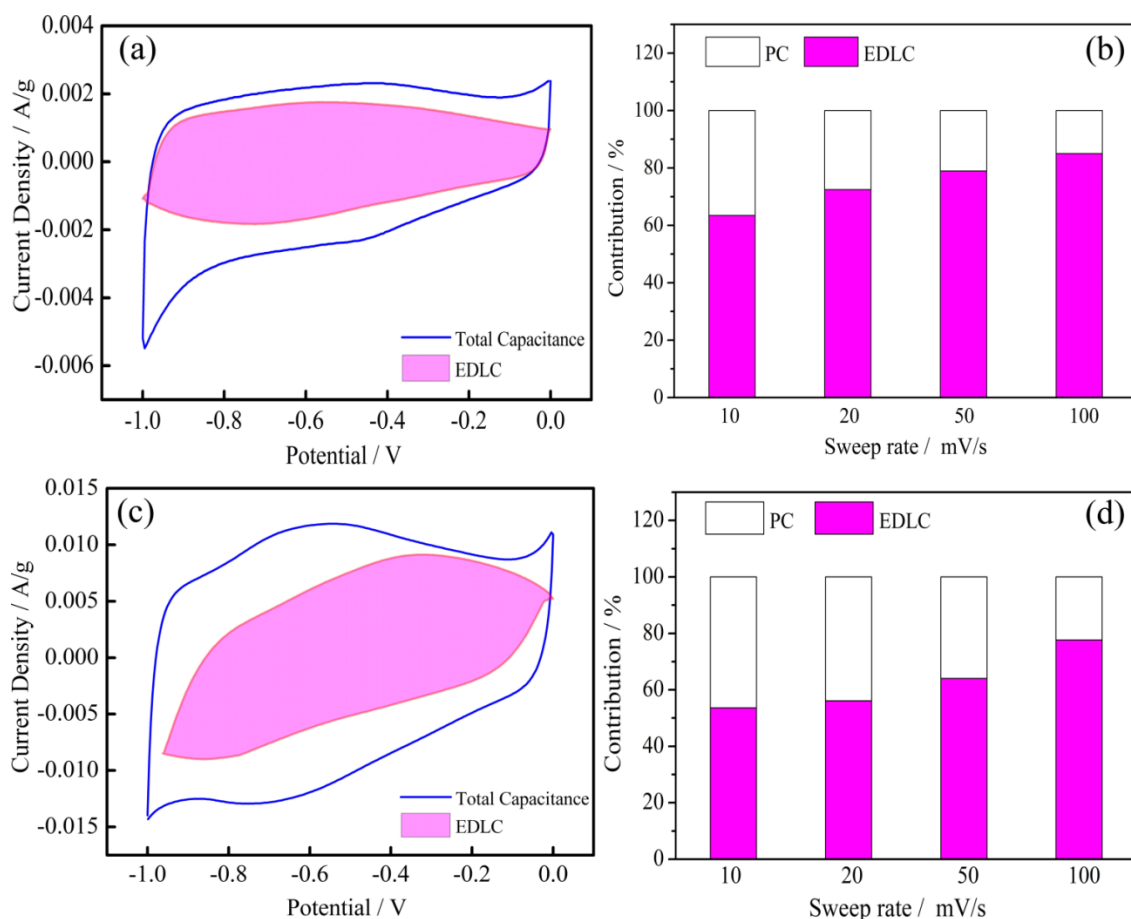


Figure 6. The EDLC contributions of (a) HCNFs-1 and (b) HCNFs-2 at 10 mV/s and the EDLC and PC contributions of (c) HCNFs-1 and (d) HCNFs-2 at different scan rates.

It is important to understand the capacitive behaviour of samples HCNFs-1 and HCNFs-2, which are expected to have both PC and EDLC. The respective contribution of the EDLC and PC can be calculated by the Dunn method (5) [44, 45]:

$$i(V) = k_1 v + k_2 v^{1/2} \quad (5)$$

The voltage (V) of current (i) corresponding to a certain sweep rate (v) is the sum of the EDLC ($k_1 v$) and the PC ($k_2 v^{1/2}$). The EDLC is mainly derived from carbon matrices, while the PC comes from surface oxygen-containing functional groups. The proportion of the EDLC can be obtained by calculating the integral of the area. As shown in the pink part of Figure 6a and c, the percentages of the capacitive contribution to the total capacity are 64.5% and 53.5% at a scan rate of 10 mV/s, respectively. For samples HCNFs-1 and HCNFs-2, the proportion of the EDLC contribution increases with scan rate in Figure 6b and d.

4. CONCLUSION

To further improve their capacitance performance, HCNFs were oxidized by HNO_3 treatment and the modified Hummers method to increase the oxygen-containing functional groups and specific

surface area on their surface. The oxidation process was highly effective in introducing oxygen-bearing functional groups without degrading the structural integrity of the surface of the HCNFs. Following this treatment, the S_{BET} and V_t of HCNFs-1 and HCNFs-2 were greatly increased. Moreover, a large quantity of O–H and COOH was present on the surfaces of samples HCNFs-1 and HCNFs-2 from Faradaic redox reactions in the KOH and greatly enhanced the specific capacitance, which created novel EDLC and PC coexisting supercapacitor materials. The capacitance of sample HCNFs-2 (143.6 F/g) was much higher than that of the pristine HCNFs (10.7 F/g) and sample HCNFs-1 (65.5 F/g) at a scan rate of 1 A/g.

ACKNOWLEDGMENTS

This research was financially supported by the Opening Project of Sichuan University of Science and Engineering, Material Corrosion and Protection Key Laboratory of Sichuan province (2020CL02) and the Basic Applied Research Projects in Sichuan Province (2019YJ0479).

References

1. R. Vijayan, A. Ghazinezami, S. R. Taklimi, M. Y. Khan and D. Askari, *Compos. Pt. B-Eng.*, 156 (2019) 28.
2. N. Kadhim, Y. Mei, Y. Wang, Y. Li, F. Meng, M. Jiang and Z. Zhou, *Polymers*, 10 (2018) 1103.
3. H. Yang, B. Li, R. Cui, R. Xing and S. Liu, *J. Nanopart. Res.*, 19 (2017) 354.
4. Q. Zhang, M. Fu, H. Lu, X. Fan, H. Wang, Y. Zhang and H. Wang, *Sens. Actuator B-Chem.*, 296 (2019) 126667.
5. H. Tang, X. Jian, B. Wu, S. Liu, Z. Jiang, X. Chen, W. Lv, W. He, W. Tian, Y. Wei, Y. Gao, T. Chen and G. Li, *Pt. B-Eng.*, 107 (2016) 51.
6. K. Li, H. Sun, X. Zhang, S. Zhang, H. Dong, C. Zhu and Y. Chen, *Mater. Des.*, 186 (2020) 108290.
7. A. Childress, K. Ferri and A. M. Rao, *Carbon*, 140 (2018) 377.
8. Q. Zeng, H. Tian, J. Jiang, X. Ji, D. Gao and C. Wang, *RSC Adv.*, 7 (2017) 7375.
9. H. Luo, H. Lu and J. Qiu, *J. Electroanal. Chem.*, 828 (2018) 24.
10. F. Wu, J. Du, C. Liu, L. Li and H. Cheng, *New Carbon Mater.*, 19 (2004) 81.
11. Y. Lin, M. R. Funk, C. J. Campbell, J. Kim, X. Han, S. D. Lacey, H. Xie, L. Hu and J. W. Connell, *Adv. Funct. Mater.*, 27 (2017) 1700762.
12. Y. Zheng, W. Zhao, D. Jia, L. Cui and J. Liu, *Chem. Eng. J.*, 364 (2019) 70.
13. L. Jiang, J. Wang, X. Mao, X. Xu, B. Zhang, J. Yang, Y. Wang, J. Zhu and S. Hou, *Carbon*, 111 (2017) 207.
14. L. Guo, Z. Luo, Y. Zhao, J. Guo, M. Zhu, K. Luo and A. Z. Huang, *Int. J. Electrochem. Sci.*, 14 (2019) 11081.
15. W. Chen, Z. Zhao and X. Yu, *Electrochim. Acta*, 341 (2020) 136044.
16. N. Phattharasupakun, J. Wutthiprom, P. Suktha, P. Iamprasertkun, N. Chanlek, C. Shepherd, E. Hadzifejzovic, M. G. Moloney, J. S. Foord and M. Sawangphruk, *Electrochim. Acta*, 238 (2017) 64.
17. Y. He, Y. Zhang, X. Li, Z. Lv, X. Wang, Z. Liu and X. Huang, *Electrochim. Acta*, 282 (2018) 618.
18. Y. Chen, Z. Zhang, Z. Huang and H. Zhang, *Int. J. Hydrog. Energy*, 42 (2017) 7186.
19. Y. Lee, K. Chang and C. Hu, *J. Power Sources*, 227 (2013) 300.
20. R. Singhal and V. Kalra, *J. Mater. Chem. A*, 3 (2015) 377.
21. H. Cao, X. Peng, M. Zhao, P. Liu, B. Xu and J. Guo, *RSC Adv.*, 8 (2018) 2858.
22. Y. Jin, J. Chen, Q. Fu, B. Li, H. Zhang and Y. Gong, *Appl. Surf. Sci.*, 324 (2015) 438.

23. W. S. Hummers and R. E. Offeman, *J. Am. Chem. Soc.*, 80 (1958) 1339.
24. H. Deng, M. Zhu, T. Jin, C. Cheng, J. Zheng and Y. Qian, *Int. J. Electrochem. Sci.*, 15 (2020) 16.
25. Y. J. Oh, J. J. Yoo, Y. I. Kim, J. K. Yoon, H. N. Yoon, J. Kim and S. B. Park, *Electrochim. Acta*, 116 (2014) 118.
26. P. Xi, T. Zhao, L. Xia, D. Shu, M. Ma and B. Cheng, *Sci. Rep.*, 7 (2017) 40390.
27. C. Yoon, D. Long, S. Jang, W. Qiao, L. Ling, J. Miyawaki, C. Rhee, I. Mochida and S. Yoon, *Carbon*, 49 (2011) 96.
28. Z. Wang, Z. Wu, G. D. Benedetto, J. L. Zunino III and S. Mitra, *Carbon*, 91 (2015) 103.
29. G. Wang, R. Liang, L. Liu and B. Zhong, *Electrochim. Acta*, 115 (2014) 183.
30. L. Han, L. Zhang, H. Wu, H. Zu, P. Cui, J. Guo, R. Guo, J. Ye, J. Zhu, X. Zheng, L. Yang, Y. Zhong, S. Liang and L. Wang, *Adv. Sci.*, 6 (2019) 1900006.
31. S. K. Park, Q. Mahmood and H. S. Park, *Nanoscale*, 5 (2013) 12304.
32. L. Wang, C. Li, F. Gu and C. Zhang, *J. Alloys Compd.*, 473 (2009) 351.
33. V. Thirumal, A. Pandurangan, R. Jayavel, S.R. Krishnamoorthi and R. Ilangovan, *Curr. Appl. Phys.*, 16 (2016) 816.
34. J. Cherusseri, R. Sharma and K. K. Kar, *Carbon*, 105 (2016) 113.
35. Y. Fang, B. Luo, Y. Jia, X. Li, B. Wang, Q. Song, F. Kang and L. Zhi, *Adv. Mater.*, 24 (2012) 6348.
36. C. Chen, Q. Zhang, X. Zhao, B. Zhang, Q. Kong, M. Yang, Q. Yang, M. Wang, Y. Yang, R. Schlögl and D. Su, *J. Mater. Chem.*, 22 (2012) 14076.
37. M. Kim and J. Kim, *ACS Appl. Mater. Interfaces*, 6 (2014) 9036.
38. J. Yang and S. Gunasekaran, *Carbon*, 51 (2013) 36.
39. C. Zheng, X. Zhou, H. Cao, G. Wang and Z. Liu, *J. Mater. Chem. A*, 3 (2015) 9543.
40. P. L. Taberna, P. Simon and J.F. Fauvarque, *J. Electrochem. Soc.*, 150 (2003) A292.
41. H. X. Zhang, V. V. Bhat, N. C. Gallego and C. I. Contescu, *ACS Appl. Mater. Interfaces*, 4 (2012) 3239.
42. C. Huang, Y. Wu, C. Hu and Y. Li, *J. Power Sources*, 172 (2007) 460.
43. L. Liu, Y. Chen, Y. Xie, P. Tao, Q. Li and C. Yan, *Adv. Funct. Mater.*, 28 (2018) 1801989.
44. J. Wang, J. Polleux, J. Lim and B. Dunn, *J. Phys. Chem. C*, 111 (2007) 14925.
45. V. Augustyn, P. Simon and B. Dunn, *Energy Environ. Sci.*, 7 (2014) 1597.

© 2020 The Authors. Published by ESG (www.electrochemsci.org). This article is an open access article distributed under the terms and conditions of the Creative Commons Attribution license (<http://creativecommons.org/licenses/by/4.0/>).